Phosphatidic Acid Accumulates at Areas of Curvature in Tubulated Lipid Bilayers and Liposomes

Broderick L. Bills, Michelle K. Knowles*

Department of Chemistry and Biochemistry, University of Denver, Denver, CO 80210 Molecular and Cellular Biophysics Program, University of Denver, Denver, CO 80210 * corresponding author

Keywords: Phosphatidic acid, membrane curvature, tubules

ABSTRACT:

Phosphatidic acid (PA) is a signaling lipid that is produced enzymatically from phosphatidylcholine (PC), lysophosphatidic acid, or diacylglycerol. Compared to PC, PA lacks a choline moiety on the headgroup, making the headgroup smaller than that of PC and PA, and PA has a net negative charge. Unlike the cylindrical geometry of PC, PA, with its small headgroup relative to the two fatty acid tails, is proposed to support negatively curved membranes. Thus, PA is thought to play a role in a variety of biological processes that involve bending membranes, such as the formation of intraluminal vesicles in multivesicular bodies and membrane fusion. Using supported tubulated lipid bilayers (STuBs), the extent to which PA localizes to curved membranes was determined. STuBs were created via liposome deposition with varying concentrations of NaCl (500 mM to 1 M) on glass to form supported bilayers with connected tubules. The location of fluorescently labeled lipids relative to tubules was determined by imaging with total internal reflection or confocal fluorescence microscopy. The accumulation of various forms of PA (with acyl chains of 16:0-6:0, 16:0-12:0, 18:1-12:0) were compared to PC and headgroup labeled phosphatidylethanolamine (PE), a lipid that has been shown to accumulate at regions of curvature. PA and PE accumulated more at tubules and led to the formation of more tubules than PC. Using large unilamellar liposomes in a dye quenching assay, the location of headgroup labeled PE was determined to be mostly on the outer, positively curved leaflet, whereas tail-labeled PA was located more on the inner, negatively curved leaflet. This study demonstrates that PA localizes to regions of negative curvature in liposomes and supports the formation of curved, tubulated membranes. This is one way that PA could be involved with curvature formation during a variety of cell processes.

INTRODUCTION:

Phosphatidic acid (PA) is a lipid that can be produced from phosphatidylcholine (PC), diacylglycerol, lysophosphatidic acid (LPA) or *de novo* from glycerol 3-phosphate or dihydroxyacetone phosphate [1,2]. The roles of PA are currently best described in plants, particularly *Arabidopsis thaliana*, where PA is involved in a wide variety of processes, from stress response and growth, acting primarily as a signaling molecule [3]. In yeast, PA is involved in sporulation and secretion [3]. In mammals, PA is involved in exocytosis, intraluminal formation, cell proliferation, signaling, tumor progression and cell differentiation [3].

Many of the roles that PA have in biology are hypothesized to be related to the geometry of PA itself. PA has been shown to regulate cellular functions by altering membrane shape locally on the plasma membrane or organelle membranes [4]. PA has an inverse conical shape when compared to PC [5]. Inverse conical shaped lipids are predicted to ease membrane bending by fitting well into negatively curved membranes, whereas conical shaped lipids, such as LPA [5] and PE with a large fluorescent dye label on the headgroup, are predicted to sort into positively curved membrane areas [6]. The presences of lipids with intrinsic membrane shape makes membrane bending easier and could also be a mechanism by which lipids are sorted [7,8].

Several studies have focused on the interplay between membrane shape and the intrinsic lipid shape. Positively curved membranes accumulated single tailed lipids, such as fluorescein-labeled hexadecanoic acid [6] and LPA [9], which are conical in shape. Interestingly, lipids with two tails also accumulate (fluorescein 1,2-dihexadecanoyl-sn-glycero-3-phosphoethanolamine, Fl-DHPE) to a higher extent [6,10]. An alternative model for lipid sorting depends on the defect sites in the bilayer that are present when a membrane bends [11]. The positively curved side has packing defect sites that, when present, allow for the insertion of hydrophobic protein motifs or lipids [10,12]. Therefore, defect sites are places in the membrane that can be stabilized by filling with lipids. Lipids with more carbons in the tails (either longer tails or two tails) have been shown to accumulate more at these sites [6,10]. This is in contrast to the concept of sorting based on the intrinsic lipid shape, and the work presented here focuses on both the role of lipid tails and the small headgroup in PA curvature membrane sorting.

To measure how lipids and proteins are recruited by or induce curved membranes, several model curved membrane assays exist, such as curved supported lipid bilayers [13], tubules [14], membrane coated nanopatterned surfaces [15–17], and small liposome-based assays [10,18]. Recently, an assay using NaCl to induce tubule formation in supported lipid bilayers (SLBs) was developed by Schenk *et al* [19]. These supported tubulated bilayers (STuBs) were used to study Sar1B, a vesicle budding protein [19], but in this study, we demonstrate that this assay is useful for measuring lipid accumulation at curvature as well. This assay was chosen partly due to the simplicity of creating the tubules but also because the tubes are connected to the flat supported bilayer, allowing the measurement of recruitment to curved regions to be directly compared to flat areas in the same measurement.

In this work, STuBs were used to measure the recruitment of PA to curvature and to determine if PA supports membrane curvature formation and if PA accumulates at regions of curvature. STuBs were created from POPC, DOPE-PEG and a fluorescent lipid (either PA, PC or PE) and imaged using confocal and TIRF microscopies. From image data, the number of tubes per area and the

intensity of dye labeled lipid per tube were quantified relative to the flat areas of the same samples. As an alternative, extruded large unilamellar liposomes were measured in bulk and the accessibility of the dye to quenching agents was assessed to determine which leaflet accumulated PA. Our results demonstrate that PA stabilizes curvature and prefers negatively curved areas relative to PC controls.

METHODS

Liposome and STuBs Assembly: Lipids were mixed in chloroform to specified concentrations using glass syringes for a total of 250 nmol. Chloroform was evaporated using nitrogen and vacuum. Lipids were resuspended in 2 mL of buffer containing 140 mM KCl, 20 mM HEPES and varying concentrations of NaCl at pH 7.4. The solution was probe sonicated for 5 min on ice. For SLBs, 8 well dishes were cleaned by submerging in 0.1% SDS for 1 hour, followed by 1% bleach overnight, then 100 µL of 2% Hellmanex was added to each well for one hour. Afterwards, wells were rinsed three times in buffer containing 140 mM KCl, 20 mM HEPES and varying concentrations of NaCl at pH 7.4. 100 µL of liposome stocks were deposited per well in 8 well dishes and incubated at 37°C for 1 hour. SLBs were then imaged immediately. Lipids used in this study include 1-palmitoyl-2-oleoyl-glycero-3-phosphocholine (POPC, Avanti Polar Lipids, 1,2-dioleoyl-sn-glycero-3-phosphoethanolamine-N-[methoxy(polyethylene 2000] (DOPE-PEG, Avanti Polar Lipids, 880234), Marina Blue- 1,2-dihexadecanoyl-snglycero-3-phosphoethanolamine (MB-DPPE, ThermoFisher, M12652), 1,1'-dioctadecyl-3,3,3',3'tetramethylindodicarbocyanine, 4-chlorobenzenesulfonate salt (DiD, ThermoFisher, D7757), 1,1'dioctadecyl-3,3,3',3'-tetramethylindocarbocyanine perchlorate (DiI, ThermoFisher, D282), 1palmitoyl-2-{6-[(7-nitro-2-1,3-benzoxadiazol-4-yl)amino]hexanoyl}-sn-glycero-3-phosphate (16:0 6:0-NBD PA, Avanti Polar Lipids, 810173), 1-palmitoyl-2-{12-[(7-nitro-2-1,3benzoxadiazol-4-yl)amino]dodecanoyl}-sn-glycero-3-phosphate (16:0 12:0-NBD PA Avanti Polar Lipids, 810174), 1-oleoyl-2-{12-[(7-nitro-2-1,3-benzoxadiazol-4-yl)amino]dodecanoyl}sn-glycero-3-phosphate (18:1 12:0-NBD PA, Avanti Polar Lipids, 810176), 1-oleoyl-2-[12-[(7nitro-2-1,3-benzoxadiazol-4-yl)amino|dodecanoyl]-sn-glycero-3-phosphocholine (18:1 NBD PC, Avanti Polar Lipids, 810133), and 1,2-dipalmitoyl-sn-glycero-3-phosphoethanolamine-N-(7-nitro-2-1,3-benzoxadiazol-4-yl) (NBD-DPPE, Avanti Polar Lipids, 810144). Liposomes contained 98% POPC, 1% DOPE-PEG and 1% NBD-labeled lipid. SLBs used for FRAP contained 96.9% POPC 1% DOPE-PEG, 2% MB-DPPE and 0.1% DiD. SLBs used for TIRF contained 98% POPC, 1% DOPE-PEG, and 1% NBD-labeled lipid. MB-DPPE concentration was 2%, the same as past work [16], and NBD labeled PA lipids were used at a concentration relevant to what is observed in cells [20,21]. POPC concentration was adjusted to accommodate the difference. All lipids were purchased from Avanti Polar Lipids (Alabaster, Alabama, USA), except for MB-DPPE, Dil and DiD, which were purchased from ThermoFisher. Dil was used in TIRF measurements and DiD was used for confocal measurements of the membrane tubule size due to the excitation wavelengths available on different microscopes. MB-DPPE was used for measuring fluidity.

Fluorescence Recovery After Photobleaching (FRAP): FRAP was performed on a point-scanning confocal microscope (Olympus Fluoview 3000) to test fluidity of bilayers and connectivity of tubules. The FRAP region was a 60 pixel diameter (6.01 μm) circle. A 640 nm laser was used for DiD and a 405 nm laser for MB-DPPE. The imaging rate was 2.17 seconds per frame during 2-color imaging. 3 frames were taken prior to bleaching, then FRAP region was bleached for 1s, followed by 45 frames for recovery. FRAP occurred at room temperature 20-22°C. FRAP data was corrected for photobleaching and normalized to the average of the pre-

bleach frames as described in previous work [6,16]. Graphpad Prism was used for plotting, fitting and t-testing.

Total Internal Reflection Fluorescence Microscopy: STuBs samples were imaged immediately after assembly. Two color imaging data were taken with a 60x (1.49 NA) objective followed by a 2.5x magnifying lens to obtain a magnification that is 0.109 μm/pixel on the detector (EMCCD, Andor iXon897). A DualView (Optical Insights) was used to split the red and green fluorescence (565LP dichroic with 525/50 and 605/75 emission filters, Chroma Technologies) into separate channels onto the camera. Movies were taken at 1 frame/second using Micromanager [22].

For image analysis, the red and green images were aligned using 200 nm carboxylate modified, vellow-green fluospheres (ThermoFisher, F8811) and home-built alignment code in MATLAB, as used previously [23,24]. These nanoparticles (diameter = 200 nm) were also used to identify the diffraction limit of the TIRF in full width half max (FWHM) calculations [21,22]. Tubule positions were located by bandpass filtering with 9 pixels followed by spot finding with a pixel size of 5 and a variable threshold. All spot-finding code was initially written in IDL [25], then made available in MATLAB [26]. Radial plots were calculated as described previously [27], and the intensity from each peak was normalized to the intensity ~500nm away. These plots were used to calculate the FWHM of tubules based on the max intensity and the flat intensity, also ~500nm away. The FWHM was called the diameter of the tubule for all plots. Intensity ($\Delta F/S$) measurements were calculated, where $\Delta F = \text{circle} - \text{annulus}$. The average intensity of a circle with a 5-pixel diameter and the intensity of an annulus 1 pixel wide, 7 pixels from the peak, were used (Fig. S1). This is normalized by S where S = annulus- background; the background was defined as the intensity of a membrane with no fluorophores present. This has been described in detail previously [23]. Longer length tubules were occasionally noted as others observed previously [19]. These tubules are typically disconnected from the bilayer and rare. Therefore, these were not used in measurements for this paper. All analysis was performed in MATLAB and code will be made available upon request. All statistical testing was performed in GraphPad Prism.

Fluorimetry: NBD labeled liposomes in 2.5 mL buffer (140 mM KCl, 20 mM HEPES and 15mM NaCl at pH 7.4) were extruded through 100 nm filters and put in a 1 cm quartz cuvette with a stir bar. 250 μL of 0.1 mM dithionite was added after 30 s. Readings were taken on a Cary Eclipse once per second, with 0.1 second exposure, an excitation wavelength of 463 nm and emission of 533 nm. Excitation and emission slit widths were variable depending on intensity of samples, between 5 and 20 nm.

RESULTS:

The formation of STuBs depends on NaCl concentration. To determine what concentration of NaCl reliably formed tubules, SLBs were formed using 96.9% POPC, 1% DOPE-PEG, 2% Marina Blue-DPPE and 0.1% DiD at varying concentrations of NaCl (Fig. 1A). The lowest and highest concentration were chosen to replicate the original STuBs study [19]. This combination of lipids was intended to be a simple mixture that mimics the plasma membrane and includes PEGylated lipids to cushion the bilayer from the glass surface [28] and mimic the crowded cellular environment [29]. Increasing the concentration of NaCl reproducibly induced formation of more tubules (Figs. 1A and 1B). On rare occasion, long tubules formed as seen in other labs[19], but were not included in our analyses due to their rarity and their shapes complicating analysis. Instead,

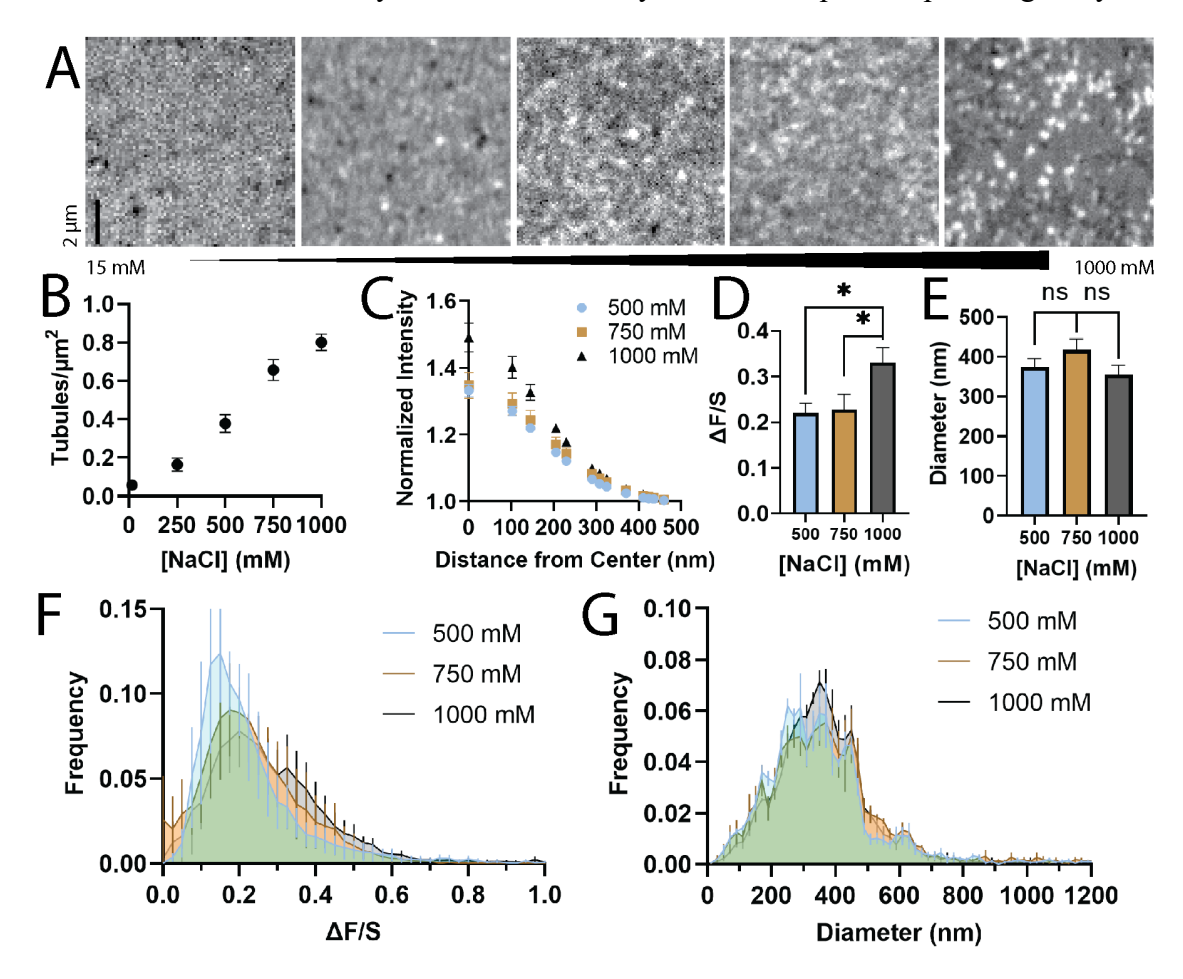


Figure 1: Tubules form in the presence of 500-1000 mM NaCl. Lipid tubules were characterized using 0.1% DiD as a lipid marker. Increasing concentration of NaCl increases number of tubules per area. A) Tubules were imaged using confocal microscopy. [NaCl] from top to bottom (mM): 15, 250, 500, 750, 1000. All images are autoscaled. B) DiD labeled tubule density as a function of NaCl concentration. C) Radial plots of intensity of DiD at 500 mM (blue circles), 750 mM (brown squares) and 1000 mM (black triangles) normalized to intensity at 951 nm from center. D) Average intensity of lipids at sites of tubules for different [NaCl], displayed as $\Delta F/S$, a function of tubule intensity and surrounding intensity. E) Average size in nm at [NaCl] of 500, 750 and 1000 mM. All error bars are SEM (n = 9). F) The distribution of intensities of single tubules and G) The distribution of the diameter, as measured from the FWHM of the imaged tubule. Error bars in histograms are SEM from three days.

smaller tubules were measured and are fluid with the rest of the bilayer (Fig. S2), which suggests they are connected structures, rather than liposomes. These tubule structures recovered to the same extent as the flat regions of the membrane (Fig. S2). The tubules diffraction limited (Figs. 1A and 1E), but the intensity of the varied tubules with NaC1 concentration (Fig. 1D) based on measurements of $\Delta F/S$, described in Fig. S. Specifically, tubules assembled in 1000 mM NaCl were significantly more intense than those at 500 or 750 mM (Fig. 1D), while differences in FWHM values of tubules at any [NaCl] were not significant (Fig. 1E). This suggests that tubules may be larger with higher concentration of NaCl. Since single tubules can be observed in this assay, the distribution of intensity and sizes can also be quantified (Fig distributions The 1G). intensity ($\Delta F/S$) and the tubule size (FWHM) is similar for tubules prepared with 500, 750 or 1000 mM NaCl.

PA and DPPE Form More Tubules Than PC. To determine if lipids with intrinsic curvature affected STuBs formation or accumulate in certain regions, tail labeled PA (NBD-PA) and headgroup

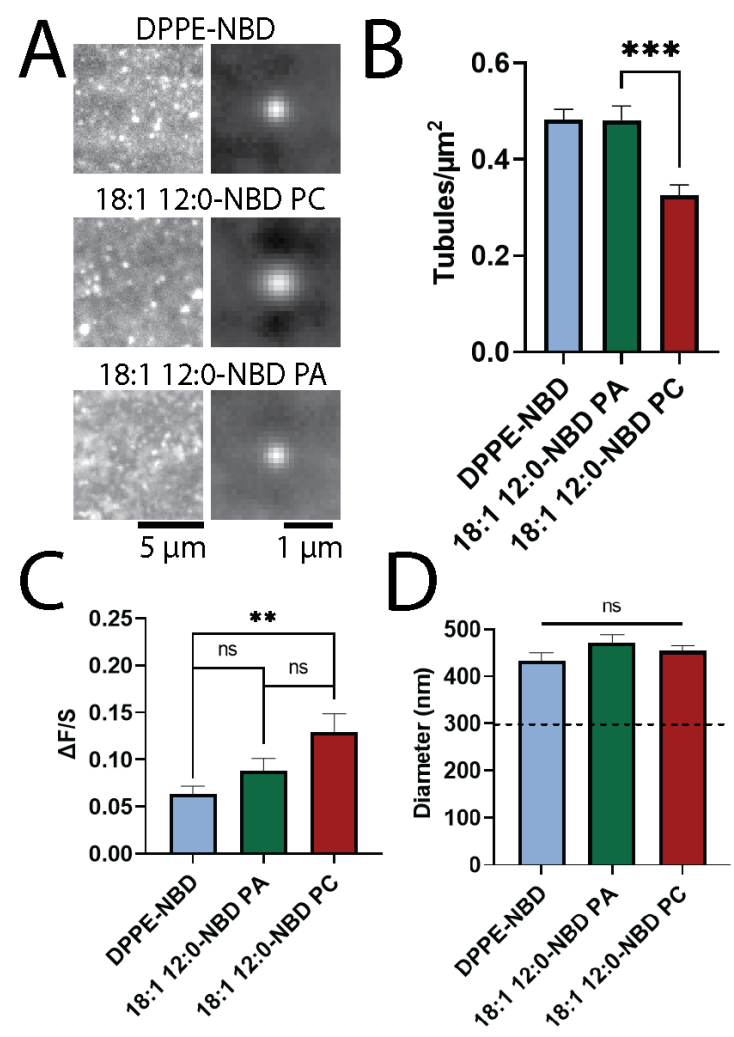


Figure 2: Tubulated lipid bilayers with PA and DPPE induce more tubule formation than PC. A) Examples of bilayers with 18:1 12:0-NBD PA (top), 18:1 12:0-NBD PC (middle) and DPPE-NBD (bottom), with examples of STuBs (left) and averaged tubules (right). B) Average tubule density of bilayers with respective lipids. C) Average $\Delta F/S$ of lipids. D) Average diameter (FWHM) of lipids. On our microscope, the average FWHM of diffraction-limited 200 nm green polystyrene nanoparticles is 296 nm (dashed line). Error bars are SEM. n = 12 membranes between 3 days.

labeled DPPE (DPPE-NBD) were incorporated separately into the STuBs. In this experiment, all lipids were identical except the ones labeled on the axis in Figure 2. Membranes were formed in 1000 mM NaCl buffer, using 98% POPC, 1% DOPE-PEG, and 1% either DPPE-NBD, (18:1 12:0)-NBD-PC, or (18:1 12:0)-NBD-PA then imaged using TIRF microscopy. Example images are shown alongside an average of the tubule regions for each lipid combination (Fig. 2A). In this experiment, PC acted as a negative control, while DPPE-NBD was a positive control because it sorts into positively curved membranes [6,30]. The NBD-PA produced more tubules than NBD-

PC and as many as DPPE-NBD (Fig. 2B). This supports the hypothesis that PA affects membrane curvature formation. Next, the intensity of the tubules was evaluated to determine if tubules contained higher amounts of the NBDlabeled lipids. The intensity $(\Delta F/S)$ varied as a function of the lipid headgroups with **NBD-PA** tubules being dimmer than NBD-PC tubules (Fig. 2C). The higher intensity (Fig 2C) suggests that either more PC is present in tubules, relative to PA and DPPE, or tubules are larger when NBD-PC is present. However, no significant difference in the tubule diameter (FWHM) was observed between PA, PC or PE (Fig. 2D). Therefore, more PC is likely present on the tubules.

Longer fatty acid chains support tubule formation. Although the headgroup of a lipid likely plays a key role in determining localization to curved membranes [5–9], the acyl chains have also been shown to affect the overall geometry and sorting on different membranes shapes [6,10]. To determine the role

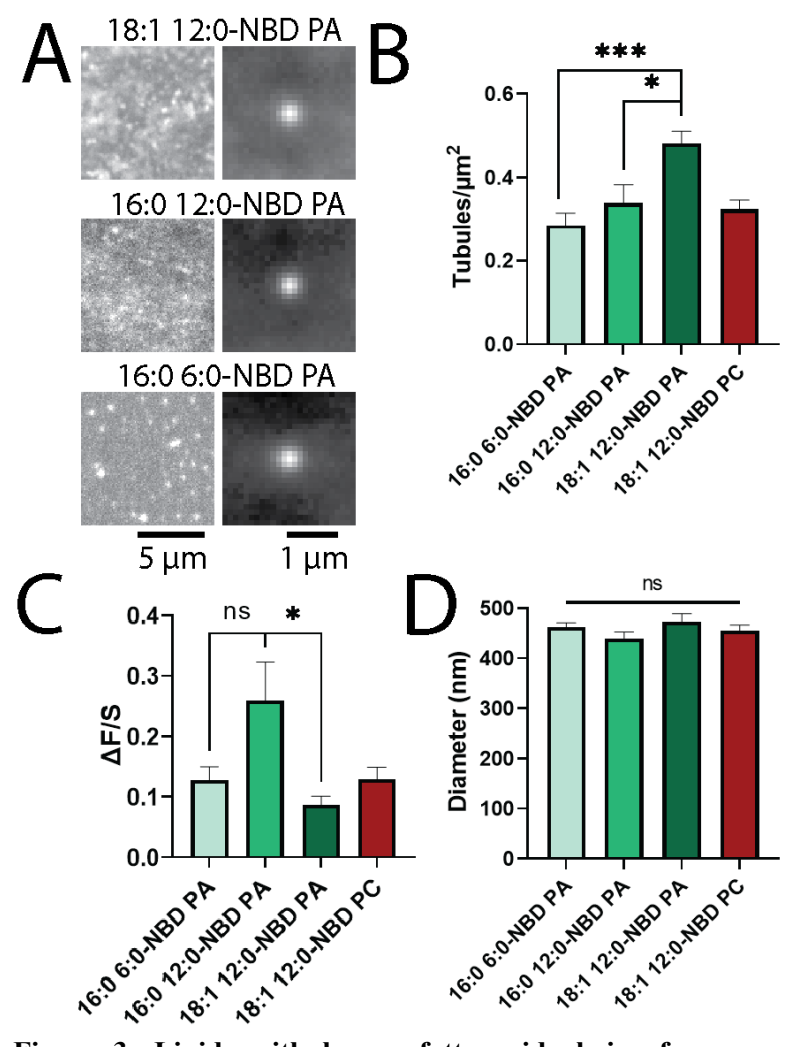


Figure 3: Lipids with longer fatty acid chains form more tubules. A) Examples of tubules containing 1% fatty acid-labeled PA. 18:1 12:0-NBD PA (top), 16:0 12:0-NBD PA (middle), 16:0 6:0-NBD PA (bottom). B) Tubule density of bilayers with respective lipids. C) Average $\Delta F/S$ values of lipids. D) Average FWHM of lipids. All differences are not significant in D. Error bars are SEM. n = 12 membranes between 3 days.

that the acyl chains play in lipid sorting, several PAs with modified tails were compared for their ability to sort into curved membranes and support the formation of tubules. Specifically, two fully saturated NBD-PAs (16:0 12:0-NBD PA and 16:0 6:0-NBD PA) were used in addition to the monounsaturated 18:1 12:0-NBD PA (Fig. 3). The presence of 18:1 12:0 NBD PA led to more tubule formation than 16:0 12:0 NBD PA and 16:0 12:0 NBD PA led to more tubule formation than 16:0 6:0 PA, showing a trend with the size of the lipid tails (Figs. 3A and B). PA supports the formation of more tubules when more carbons are present in the fatty acid chains, as shown by the higher density of tubules with PA as compared to PC with identical acyl chains (Fig. 3B). Unlike the density of tubules, the intensity of tubules (Fig 2C) did not trend with the number of carbons in the fatty acyl chains. Instead, tubules with 16:0 12:0-NBD PA appear brighter than either 16:0 6:0-NBD-PA or 18:1 12:0-NBD PA (Fig. 3C); however, the variation observed in tubule intensities

was large for all tubules. The size of the tubules formed did not vary as a function of the fatty acid tail, with no significant difference in FWHM of tubules noted between PAs (Fig. 3D). Overall, this suggests that longer acyl chains and the incorporation of a bent, unsaturated tail on PA lipids can enhance the formation of membrane curvature, but the acyl tails do not affect the overall size distribution of the tubules that form.

Dithionite quenching of NBD reveals PA localization to negative curvature. The presence of PA enhances tubule formation, but it is not clear from imaging of STuBs which leaflet PA sorts into. To determine if PA prefers the inner leaflet (negative curvature) or the outer leaflet (positive curvature), a dithionite quenching assay was performed with liposomes extruded through a 100 nm filter. Typically the extrusion process yields a distribution of liposomes sizes ranging from approximately 50-150 nm [10]. Dithionite quenches NBD fluorescence [31–33]; however, dithionite does not usually penetrate through a synthetic lipid barrier. Therefore, the outer leaflet is quenched preferentially. Figure 4 shows that dithionite quenched DPPE-NBD, a positive curvature sorting lipid, to a greater extent that NBD-PC. This suggests a greater localization to the

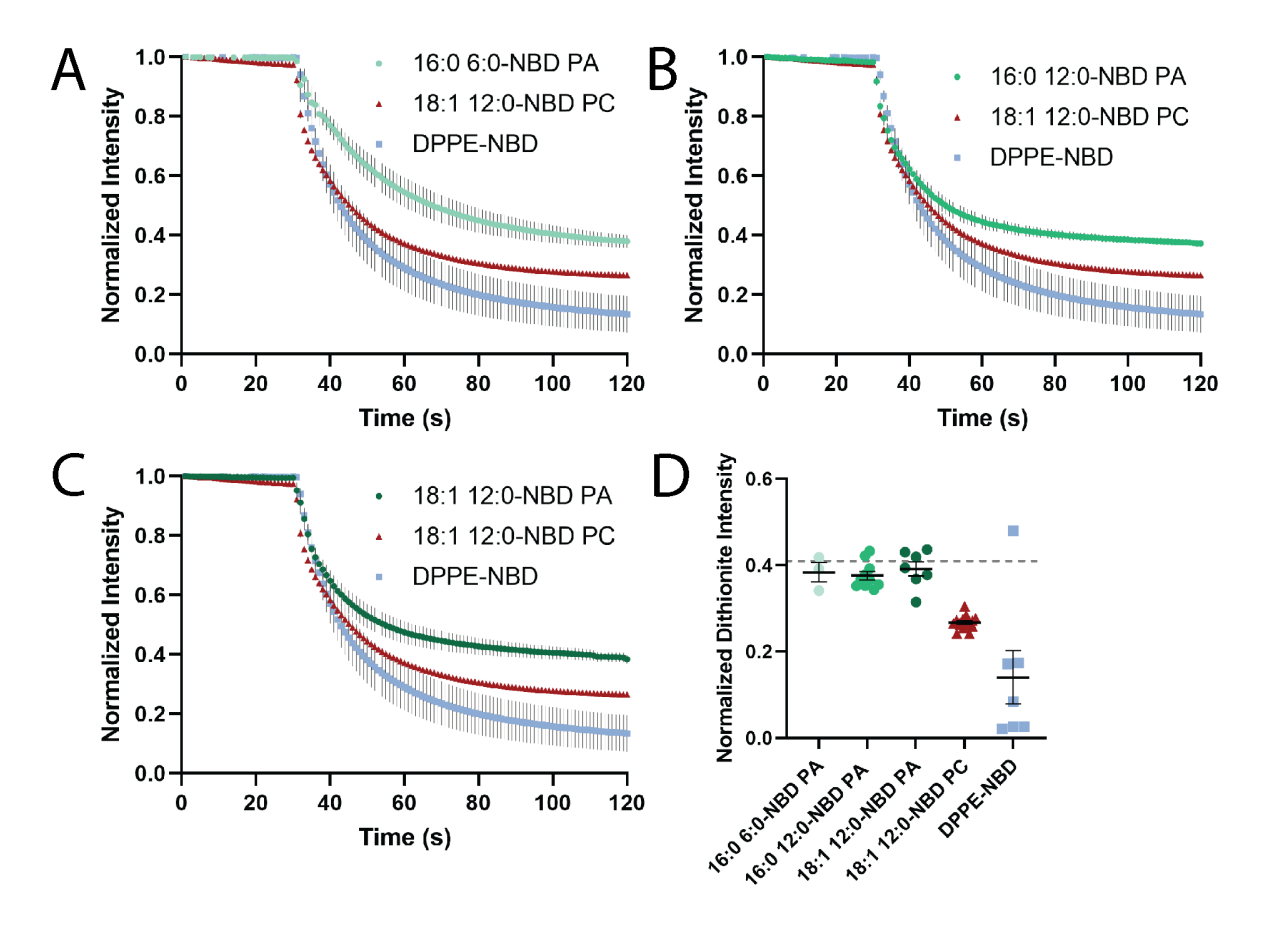


Figure 4: PA localizes to negative curvature in a liposome-based dithionite assay. Liposomes containing 98% POPC, 1% DOPE-PEG and 1% NBD-labeled lipid were extruded through 100 nm filters and fluorescence was measured in a fluorimeter. After 30 s, dithionite was added. A-C:the fluorescence traces over time. D: Normalized intensity after addition of dithionite. Dashed line: theoretical intensity if only the outer leaflet were quenched and liposomes were symmetric, accounting for surface area and dilution. Error bars are SEM; error on PC was smaller than the data points. For all PAs, p < 0.0005 (***) for PC and p < 0.05 (*) for DPPE-NBD.

outer, positively curved leaflet. Conversely, all NBD-PAs tested quenched to a lesser extent, supporting a localization to the negatively curved leaflet (Fig 4A-D). Melittin was used to form pores in the vesicles to quench the remaining inner leaflet NBD molecules (Fig S3) [6,34]. The fatty acid tails made no difference in the quenching assay (Fig 4D), suggesting that all PAs tested were similarly sorted to the interior of the liposomes.

DISCUSSION

In this work, a new membrane curvature assay that leads to the formation of tubules protruding from a supported lipid bilayer [19] has been used to determine if PA prefers and/or stabilizes curved membranes. Although STuBs are simple to form and allow for the visualization of lipids at regions with and without curvature simultaneously, there are challenges. To form STuBs, much higher concentrations of NaCl than is physiologically relevant are needed. Additionally, the readout of the assay is fluorescence, necessitating fluorophores on lipids. Studies using NMR experiments [32] and MD simulations [33] suggest that acyl NBD labels can bend towards the water interface. This likely complicates NBD quenching assays (Fig 4) and could affect localization. To account for dye labeling effects, the use of an identically labeled PC as a control was essential for comparison. Despite these challenges, the use of fluorescent lipids also provides advantages. Fluorescence assays have high signal to noise, allowing lower concentrations of lipids to be assessed, down to single molecules level concentrations [16]. In this work, the sensitivity of the assay allows PA curvature localization to be probed at a concentration that is similar to the amount of PA in mammalian and plant cells [20,21].

The formation of STuBs is straightforward and the addition of 500-1000 mM NaCl reliably formed tubular structures (Figs. 1A and B), similar to what others have observed [19]. These structures have varying diameters and intensity (Figs. 1C-E), which provides a method to observe localization of dye labeled lipids to varying curvatures. The wide distribution of tubule sizes (Fig. 1G) provides an advantage over previous work using a nanoparticle templated supported lipid bilayer [16], which contains only one size per sample as determined by the template choice. In the STuBs assay flat regions are also present and in continuum with curved membranes (Fig. S2), which allows for a direct comparison to regions with curvature, overcoming a limitation of liposome-based curvature sensing methods [10]. By having flat regions present, slight variations in the fluorescent lipid content when preparing STuBs or in microscopy, such as laser power, are internally corrected.

The STuBs assay was used to determine the sorting of phospholipids at curvature relative to flat regions and whether certain lipids could aid in curvature formation. From TIRF microscopy images, several features of the samples were quantified to determine if tail labeled PA and PC, and headgroup labeled PE affected tubule formation or were recruited to tubules. First, the density of tubules was determined to depend upon the lipid composition; lipids that support curvature (NBD-PAs and PE-NBD) led to the formation of more tubules when compared to the control, NBD-PC (Fig. 2B). Second, the accumulation of fluorescently labeled lipids at tubule sites relative to the surrounding flat regions (ΔF/S) was measured. In this measurement, NBD-PA and PE-NBD (Fig. 2C) accumulated slightly less than or similar to PC and this depended on the tails on PA (Fig 3C). Direct comparison of the role of the head group was determined by comparing PC to PA, both with 18:1 12:0 NBD labeled tails (Fig 2). PA stabilized curvature as observed in the increase in the number of tubules present (Fig 2B). However, the intensity of PA at tubule positions was slightly, but not significantly, less than PC (Fig. 2C). Meanwhile, PE-NBD both stabilized tubule formation (Fig. 2B) and was significantly less intense at tubule positions (Fig. 2C).

We hypothesized that a reduction in intensity of PE and PA relative to PC (Fig 2C), could be due to preferential localization to one leaflet, thus excluding the curvature sensing lipids from a portion of the tubule bilayer and reducing fluorescence. To test this, a fluorescence quenching assay was performed in liposomes extruded through 100 nm filters and shown in Figure 4. NBD-PAs quenched the least, followed by NBD-PC then PE-NBD. This suggests that PA is protected from dithionite, which cannot penetrate the membrane to reach the inner leaflet, PC is quenched more, whereas PE-NBD is quenched the most (about 85%) and likely preferentially sorted to the outer leaflet (Fig 4D). Overall, we conclude that both NBD-PA and PE-NBD assist with the formation or stabilization of membrane curvature with NBD-PA sorting to the inner, negatively curved leaflet and PE-NBD sorted to the outer, positively curved leaflet. The sorting of head group labeled PE to the inner, positively curved leaflet agrees with past work [5,6,9,30,37–39], although the preference for curvature of PE-NBD may depend on the acyl chains of other lipids present [40].

Curvature-based lipid sorting is often discussed in reference to the lipid headgroup, with smaller headgroups preferring negatively curved lipid membranes and larger headgroups preferring positively curved membranes. However, the fatty acyl chains present on a lipid are essential for sorting within cells [41] and on curved synthetic membranes [10], with lyso lipids showing a strong preference for positive curvature [5]. Conversely, previous studies have also demonstrated that lipids with more carbons in the acyl chains have greater preference for curvature, where two tailed lipids and longer lipid tails accumulated more at positively curved membranes[6,10]. In our past work, a lipid with two acyl chains (Fluorescein-DPPE) accumulated more at curvature than a single tailed, fluorescein labeled fatty acid (hexadecanoic acid) [6]. This suggests a mechanism that is different from the geometry of the lipid, and a "defect" site mechanism has been proposed [10-12]. n this model, the bent area in the positively curved membrane leads to the formation of packing defect sites, portrayed as a larger gap in the headgroups. This space can be filled with lipids or acylated proteins, where more carbons in the tails leads to more accumulation [10]. To test whether the tail composition affected PA accumulation, acyl-labeled PAs with varying tails were used: 16:0 12:0-NBD PA, 16:0 6:0-NBD PA and 18:1 12:0-NBD PA (Fig. 3A). PAs with shorter acyl chains formed significantly fewer tubules, with 16:0 6:0-NBD PA forming the fewest and 18:1 12:0-NBD PA forming the most (Fig. 3B). The average size of the tubules did not depend on the tails, as all lipids yielded tubules that were approximately the same diameter (Fig. 3D). However, the amount of NBD labeled lipids that accumulated at tubule positions did not trend with the acyl chain length (Fig. 3C). The saturated 16:0 12:0-NBD PA accumulated more than the unsaturated 18:1 12:0-NBD PA. This could be due to a more limited access to the positively curved leaflet, which is not supported by our data pertaining to NBD quenching within liposomes (Fig. 4D). Instead, it is useful to note that the longest lipid is also unsaturated and, thus, bent, whereas 16:0 12:0-NBD PA and 16:0 6:0-NBD PA are both saturated lipids. Therefore, interpretation of the accumulation (Fig. 3C) could also be due to differences in tail saturation, with unsaturated lipids accumulating less at tubule sites. However, more lipids should be examined in future work to develop a model based on lipid unsaturation. Overall, the longer tailed PA lipids and curvature sensing lipids (PA and PE) both support the formation of more tubules.

In a complementary but independent assay, dithionite was used to quench NBD labeled lipids to determine which leaflet of a membrane lipids prefer [31–33]. Using LUVs extruded through 100 nm pores, dithionite quenched more than 50% of all lipids tested. As a control that should not prefer curvature, NBD-PC fluorescence was measured (Fig. 4D). NBD-PC was quenched more than expected by dithionite. This could be due to accessibility of the dye [32,33] and this is in line with previous studies that show slow transport of dithionite across some membranes [31,32,40],

but disagrees with others [42]. A second reason PC is quenched more than 50% could be due to the liposome size; on small liposomes, the surface area on the outer leaflet is greater than the inner leaflet. We calculated this difference (Fig 4D, dashed line), however, and it does not account for the observed loss in fluorescence from dithionite treatment. Therefore, NBD-PC was used as a negative control to compare other lipids to because it is a lipid expected to have limited curvature preference [43]. PE-NBD was a positive control because several studies demonstrated that dyelabeled PE lipids have shown a preference for positive curvature in SLB studies and tubules extending from giant unilamellar vesicles [6,30]. However, another study in highly curved, small unilamellar vesicles (d < 100nm), only weak sorting was observed for PE-NBD, suggesting that the intrinsic shape of a lipid is not the only driving force for membrane curvature sorting [18]. The positive curvature preference we measure could be likely due to the dye on the headgroup altering its geometry or another mechanism, such as the defect site model [10]. When compared in the quenching assay, PE-NBD was quenched significantly more than NBD-PC (Fig 4D). This suggests that PE-NBD accumulated more on the outer leaflet of liposomes and was more accessible to dithionite treatment. Additionally, when compared to the NBD-PC control, PE-NBD formed more tubules (Fig. 2B), suggesting a preference for curvature and possibly a stabilization thereof. Unexpectedly, PE-NBD tubules were significantly dimmer than NBD-PC tubules (Fig. 2C). One possible explanation is that PE-NBD localizes to the positive curvature specifically, while PC may be on both leaflets and the liposome quenching assay supports this hypothesis. Meanwhile, dithionite quenched fluorescent PAs to a lesser extent in the liposome assay (Fig 4), and 18:1 12:0-NBD PA tubules were dimmer than 18:1 12:0 NBD-PC tubules, although not significantly (Fig. 2C). Following the same reasoning as above for PE, we conclude that PA is likely sorted to the inner leaflet of liposomes. In fact, all three PAs with varying tails quenched to the same value in the presences of dithionite, suggesting a similar preference for negative curvature (Fig. 4). Together, these data suggest PE-NBD predominantly localizes to the outer, positively curved leaflet of STuBs and liposomes, whereas PA labeled lipids prefer the inner, negatively curved leaflet, in agreement with others [6,30,31,39]. Overall, STuBs is a new method for measuring curvature sorting of lipids and curvature stabilization and PA and headgroup labeled PE are curvature stabilizing lipids.

REFERENCES

- Hodgkin, M.N.; Pettitt, T.R.; Martin, A.; Michell, R.H.; Pemberton, A.J.; Wakelam, M.J.O. Diacylglycerols and Phosphatidates: Which Molecular Species Are Intracellular Messengers? *Trends Biochem Sci* 1998, 23, 200–204, doi:https://doi.org/10.1016/S0968-0004(98)01200-6.
- 2. Thakur, R.; Naik, A.; Panda, A.; Raghu, P. Regulation of Membrane Turnover by Phosphatidic Acid: Cellular Functions and Disease Implications. *Front Cell Dev Biol* **2019**, 7, doi:10.3389/fcell.2019.00083.
- 3. Wang, X.; Devaiah, S.P.; Zhang, W.; Welti, R. Signaling Functions of Phosphatidic Acid. *Prog Lipid Res* **2006**, *45*, 250–278, doi:https://doi.org/10.1016/j.plipres.2006.01.005.
- 4. Rohrbough, J.; Broadie, K. Lipid Regulation of the Synaptic Vesicle Cycle. *Nat Rev Neurosci* **2005**, *6*, 139–150, doi:10.1038/nrn1608.
- 5. Kooijman, E.E.; Chupin, V.; Fuller, N.L.; Kozlov, M.M.; de Kruijff, B.; Burger, K.N.J.; Rand, P.R. Spontaneous Curvature of Phosphatidic Acid and Lysophosphatidic Acid. *Biochemistry* **2005**, 44, 2097–2102, doi:10.1021/bi0478502.

- 6. Cheney, P.P.; Weisgerber, A.W.; Feuerbach, A.M.; Knowles, M.K. Single Lipid Molecule Dynamics on Supported Lipid Bilayers with Membrane Curvature. *Membranes (Basel)* **2017**, 7, 15, doi:http://dx.doi.org/10.3390/membranes7010015.
- 7. Cooke, I.R.; Deserno, M. Coupling between Lipid Shape and Membrane Curvature. *Biophys J* **2006**, *91*, 487–495, doi:10.1529/biophysj.105.078683.
- 8. Callan-Jones, A.; Sorre, B.; Bassereau, P. Curvature-Driven Lipid Sorting in Biomembranes. *Cold Spring Harb Perspect Biol* **2011**, *3*, doi:10.1101/cshperspect.a004648.
- 9. Kooijman, E.E.; Chupin, V.; de Kruijff, B.; Burger, K.N.J. Modulation of Membrane Curvature by Phosphatidic Acid and Lysophosphatidic Acid. *Traffic* **2003**, *4*, 162–174, doi:https://doi.org/10.1034/j.1600-0854.2003.00086.x.
- 10. Hatzakis, N.S.; Bhatia, V.K.; Larsen, J.; Madsen, K.L.; Bolinger, P.Y.; Kunding, A.H.; Castillo, J.; Gether, U.; Hedegård, P.; Stamou, D. How Curved Membranes Recruit Amphipathic Helices and Protein Anchoring Motifs. *Nat Chem Biol* **2009**, *5*, 835–841, doi:10.1038/nchembio.213.
- 11. Bhatia, V.K.; Hatzakis, N.S.; Stamou, D. A Unifying Mechanism Accounts for Sensing of Membrane Curvature by BAR Domains, Amphipathic Helices and Membrane-Anchored Proteins. *Semin Cell Dev Biol* **2010**, *21*, 381–390, doi:10.1016/j.semcdb.2009.12.004.
- 12. Nuscher, B.; Kamp, F.; Mehnert, T.; Odoy, S.; Haass, C.; Kahle, P.J.; Beyer, K. α-Synuclein Has a High Affinity for Packing Defects in a Bilayer Membrane. *Journal of Biological Chemistry* **2004**, 279, 21966–21975, doi:10.1074/jbc.M401076200.
- 13. Parthasarathy, R.; Yu, C.; Groves, J.T. Curvature-Modulated Phase Separation in Lipid Bilayer Membranes. *Langmuir* **2006**, *22*, 5095–5099, doi:10.1021/la060390o.
- 14. Pucadyil, T.J.; Schmid, S.L. Real-Time Visualization of Dynamin-Catalyzed Membrane Fission and Vesicle Release. *Cell* **2008**, *135*, 1263–1275, doi:https://doi.org/10.1016/j.cell.2008.11.020.
- 15. Hanson, L.; Lin, Z.C.; Xie, C.; Cui, Y.; Cui, B. Characterization of the Cell–Nanopillar Interface by Transmission Electron Microscopy. *Nano Lett* **2012**, *12*, 5815–5820, doi:10.1021/nl303163y.
- 16. Black, J.C.; Cheney, P.P.; Campbell, T.; Knowles, M.K. Membrane Curvature Based Lipid Sorting Using a Nanoparticle Patterned Substrate. *Soft Matter* **2014**, *10*, 2016–2023, doi:10.1039/C3SM52522H.
- 17. Kabbani, A.M.; Woodward, X.; Kelly, C. v Revealing the Effects of Nanoscale Membrane Curvature on Lipid Mobility. *Membranes (Basel)* **2017**, 7, doi:10.3390/membranes7040060.
- 18. Kamal, M.M.; Mills, D.; Grzybek, M.; Howard, J. Measurement of the Membrane Curvature Preference of Phospholipids Reveals Only Weak Coupling between Lipid Shape and Leaflet Curvature. *Proceedings of the National Academy of Sciences* **2009**, *106*, 22245–22250, doi:10.1073/pnas.0907354106.
- 19. Schenk, N.A.; Dahl, P.J.; Hanna, M.G.; Audhya, A.; Tall, G.G.; Knight, J.D.; Anantharam, A. A Simple Supported Tubulated Bilayer System for Evaluating Protein-Mediated Membrane Remodeling. *Chem Phys Lipids* **2018**, *215*, 18–28, doi:https://doi.org/10.1016/j.chemphyslip.2018.06.002.

- 20. Welti, R.; Li, W.; Li, M.; Sang, Y.; Biesiada, H.; Zhou, H.-E.; Rajashekar, C.B.; Williams, T.D.; Wang, X. Profiling Membrane Lipids in Plant Stress Responses. *Journal of Biological Chemistry* **2002**, *277*, 31994–32002, doi:10.1074/jbc.M205375200.
- 21. Zech, T.; Ejsing, C.S.; Gaus, K.; de Wet, B.; Shevchenko, A.; Simons, K.; Harder, T. Accumulation of Raft Lipids in T-Cell Plasma Membrane Domains Engaged in TCR Signalling. *EMBO J* **2009**, *28*, 466–476, doi:10.1038/emboj.2009.6.
- 22. Edelstein, A.; Amodaj, N.; Hoover, K.; Vale, R.; Stuurman, N. Computer Control of Microscopes Using MManager. *Curr Protoc Mol Biol* **2010**, *92*, doi:10.1002/0471142727.mb1420s92.
- 23. Barg, S.; Knowles, M.K.; Chen, X.; Midorikawa, M.; Almers, W. Syntaxin Clusters Assemble Reversibly at Sites of Secretory Granules in Live Cells. *Proceedings of the National Academy of Sciences* **2010**, *107*, 20804–20809, doi:10.1073/pnas.1014823107.
- 24. Knowles, M.K.; Barg, S.; Wan, L.; Midorikawa, M.; Chen, X.; Almers, W. Single Secretory Granules of Live Cells Recruit Syntaxin-1 and Synaptosomal Associated Protein 25 (SNAP-25) in Large Copy Numbers. *Proceedings of the National Academy of Sciences* **2010**, *107*, 20810–20815, doi:10.1073/pnas.1014840107.
- 25. Crocker, J.C.; Grier, D.G. Methods of Digital Video Microscopy for Colloidal Studies. *J Colloid Interface Sci* **1996**, *179*, 298–310, doi:10.1006/jcis.1996.0217.
- 26. Blair, D.; Dufresne, E. The Matlab Particle Tracking Code Repository. [(Accessed on 10 June 2014)] 2005.
- 27. Alnaas, A.A.; Moon, C.L.; Alton, M.; Reed, S.M.; Knowles, M.K. Conformational Changes in C-Reactive Protein Affect Binding to Curved Membranes in a Lipid Bilayer Model of the Apoptotic Cell Surface. *J Phys Chem B* **2017**, *121*, 2631–2639, doi:10.1021/acs.jpcb.6b11505.
- 28. Diaz, A.J.; Albertorio, F.; Daniel, S.; Cremer, P.S. Double Cushions Preserve Transmembrane Protein Mobility in Supported Bilayer Systems. *Langmuir* **2008**, *24*, 6820–6826, doi:10.1021/la800018d.
- 29. Karatekin, E.; di Giovanni, J.; Iborra, C.; Coleman, J.; O'Shaughnessy, B.; Seagar, M.; Rothman, J.E. A Fast, Single-Vesicle Fusion Assay Mimics Physiological SNARE Requirements. *Proceedings of the National Academy of Sciences* **2010**, *107*, 3517–3521, doi:10.1073/pnas.0914723107.
- 30. Zhao, H.; Michelot, A.; Koskela, E.V.; Tkach, V.; Stamou, D.; Drubin, D.G.; Lappalainen, P. Membrane-Sculpting BAR Domains Generate Stable Lipid Microdomains. *Cell Rep* **2013**, *4*, 1213–1223, doi:10.1016/j.celrep.2013.08.024.
- 31. Angeletti, C.; Nichols, J.W. Dithionite Quenching Rate Measurement of the Inside—Outside Membrane Bilayer Distribution of 7-Nitrobenz-2-Oxa-1,3-Diazol-4-Yl-Labeled Phospholipids. *Biochemistry* **1998**, *37*, 15114–15119, doi:10.1021/bi9810104.
- 32. McIntyre, J.C.; Sleight, R.G. Fluorescence Assay for Phospholipid Membrane Asymmetry. *Biochemistry* **1991**, *30*, 11819–11827, doi:10.1021/bi00115a012.

- 33. Volinsky, R.; Cwiklik, L.; Jurkiewicz, P.; Hof, M.; Jungwirth, P.; Kinnunen, P.K.J. Oxidized Phosphatidylcholines Facilitate Phospholipid Flip-Flop in Liposomes. *Biophys J* **2011**, *101*, 1376–1384, doi:10.1016/j.bpj.2011.07.051.
- 34. Ladokhin, A.S.; Selsted, M.E.; White, S.H. Sizing Membrane Pores in Lipid Vesicles by Leakage of Co-Encapsulated Markers: Pore Formation by Melittin. *Biophys J* **1997**, *72*, 1762–1766, doi:10.1016/S0006-3495(97)78822-2.
- 35. Huster, D.; Müller, P.; Arnold, K.; Herrmann, A. Dynamics of Membrane Penetration of the Fluorescent 7-Nitrobenz-2-Oxa-1,3-Diazol-4-Yl (NBD) Group Attached to an Acyl Chain of Phosphatidylcholine. *Biophys J* **2001**, *80*, 822–831, doi:10.1016/S0006-3495(01)76061-4.
- 36. Loura, L.M.S.; Ramalho, J.P.P. Location and Dynamics of Acyl Chain NBD-Labeled Phosphatidylcholine (NBD-PC) in DPPC Bilayers. A Molecular Dynamics and Time-Resolved Fluorescence Anisotropy Study. *Biochimica et Biophysica Acta (BBA) Biomembranes* **2007**, *1768*, 467–478, doi:10.1016/j.bbamem.2006.10.011.
- 37. Harlos, K.; Eibl, H. Hexagonal Phases in Phospholipids with Saturated Chains: Phosphatidylethanolamines and Phosphatidic Acids. *Biochemistry* **1981**, *20*, 2888–2892, doi:10.1021/bi00513a027.
- 38. Verkleij, A.J.; de Maagd, R.; Leunissen-Bijvelt, J.; de Kruijff, B. Divalent Cations and Chlorpromazine Can Induce Non-Bilayer Structures in Phosphatidic Acid-Containing Model Membranes. *Biochimica et Biophysica Acta (BBA) Biomembranes* **1982**, *684*, 255–262, doi:https://doi.org/10.1016/0005-2736(82)90014-1.
- 39. Balch, C.; Morris, R.; Brooks, E.; Sleight, R.G. The Use of N-(7-Nitrobenz-2-Oxa-1,3-Diazole-4-Yl)-Labeled Lipids in Determining Transmembrane Lipid Distribution. *Chem Phys Lipids* **1994**, 70, 205–212, doi:10.1016/0009-3084(94)90088-4.
- 40. Mills, J.K.; Needham, D. Lysolipid Incorporation in Dipalmitoylphosphatidylcholine Bilayer Membranes Enhances the Ion Permeability and Drug Release Rates at the Membrane Phase Transition. *Biochimica et Biophysica Acta (BBA) Biomembranes* **2005**, *1716*, 77–96, doi:10.1016/j.bbamem.2005.08.007.
- 41. Mukherjee, S.; Soe, T.T.; Maxfield, F.R. Endocytic Sorting of Lipid Analogues Differing Solely in the Chemistry of Their Hydrophobic Tails. *Journal of Cell Biology* **1999**, *144*, 1271–1284, doi:10.1083/jcb.144.6.1271.
- 42. Mills, J.K.; Needham, D. Lysolipid Incorporation in Dipalmitoylphosphatidylcholine Bilayer Membranes Enhances the Ion Permeability and Drug Release Rates at the Membrane Phase Transition. *Biochimica et Biophysica Acta (BBA) Biomembranes* **2005**, *1716*, 77–96, doi:10.1016/j.bbamem.2005.08.007.
- 43. Cullis, P.R.; de Kruijff, B. Lipid Polymorphism and the Functional Roles of Lipids in Biological Membranes. *Biochimica et Biophysica Acta (BBA) Reviews on Biomembranes* **1979**, *559*, 399–420, doi:10.1016/0304-4157(79)90012-1.